ELECTRONIC SUPPLEMENTARY INFORMATION

Does Geometry Matter? Effect of Ligand Position in Bimetallic Ruthenium Polypyridines Siblings

Sofía E. Domínguez, German E. Pieslinger, Luciano Sanchez-Merlinsky and Luis M. Baraldo

Contents	Page

Structural characterization

Table S1. Crystallographic data for $[RuRuNCS](PF_6)_2.C_3H_6O$

Empirical Formula	C50 H45 F12 N11 O P2 Ru2 S
Formula weight	1340.11
T (K)	100
Crystal system	monoclinic
Space Group	P 2_1/c
a (Å)	13.480(8)
b (Å)	17.680(5)
c (Å)	22.610(4)
α (°)	90
β (°)	92.636(10)
γ (°)	90
V (Å^3)	5383(4)
Z	4
D_{calc} (mg/m^3)	1.654
Absorption coefficient (mm^{-1})	1.071
F (000)	2688.0
λ (Å)	0.82602
θ Range data collection (°)	1.700 / 26.998
Index ranges	$-15 \leq h \leq 15$
	$-21 \leq k \leq 21$
	$-28 \leq l \leq 27$
Reflections collected/unique	112992 / 9893
R_{int}	0.0408
Observed reflections [I>2σ(I)]	8792
Completeness (%)	87.3
Maximum / minimum transmission	1.000 / 0.873
Data / restraints / parameters	9893 / 39 / 748
Goodness-of-fit (GOF) on F^2	1.088
Final R-index [I>2σ(I)] / all data	0.0508 / 0.573
*w*R index [I>2σ(I)] / all data	0.1188 / 0.1224
Largest peak and hole (e A^{-3})	1.280 and -1.444
Weights, *w*	$1 / [\sigma^2(F_o^2) + (0.0240P)^2]$ where $P = (F_o^2 + 2F_c^2)^3$

Table S2. Selected Bond Distances and Angles for [RuRuNCS]$(PF_6)_2CH_3COCH_3$. and [RuRuCl]$(PF_6)_2.CH_3OH$ (extracted from Ref. 1)

bond length, Å				bond length, Å			
Ligand	Ru_{tb} moiety	**RuRuNCS**	**RuRuCl**	Ligand	Ru_{py} moiety	**RuRuNCS**	**RuRuCl**
CN	$Ru1_{tb}$-C(2)	1.981(5)	1.970(12)	NC	Ru_{py}-N(6)	1.997(5)	2.028(10)
	Ru_{tb}-N(7)	2.060(4)	2.087(8)	NCS	Ru_{py}-N(1)	2.077(5)	-
tpy	Ru_{tb}-N(8)	1.949(4)	1.951(8)	py1	Ru_{py}-N(2)	2.071(4)	2.085(11)
	Ru_{tb}-N(11)	2.068(4)	2.082(9)	py2	Ru_{py}-N(3)	2.082(4)	2.102(12)
bpy	Ru_{tb}-N(9)	2.076(4)	2.122(10)	py3	Ru_{py}-N(4)	2.071(5)	2.098(10)
	Ru_{tb}-N(10)	2.074(4)	2.093(9)	py4	Ru_{py}-N(5)	2.089(4)	2.112(13)
	bridge						
CN	C(2)-N(6)	1.173(7)	1.163(14)	NCS	N(1)-C(1)	1.11(1)	
					C(1)-S(1)	1.653(9)	
angle, degree				angle, degree			
Ru_{tb}(1)-C(2)-N(6)		175.6(5)	176.9(9)	Ru_{py}-N(6)-C(2)		179.3(4)	175.2(9)
				N(1)-C(1)-S		178.1(7)	

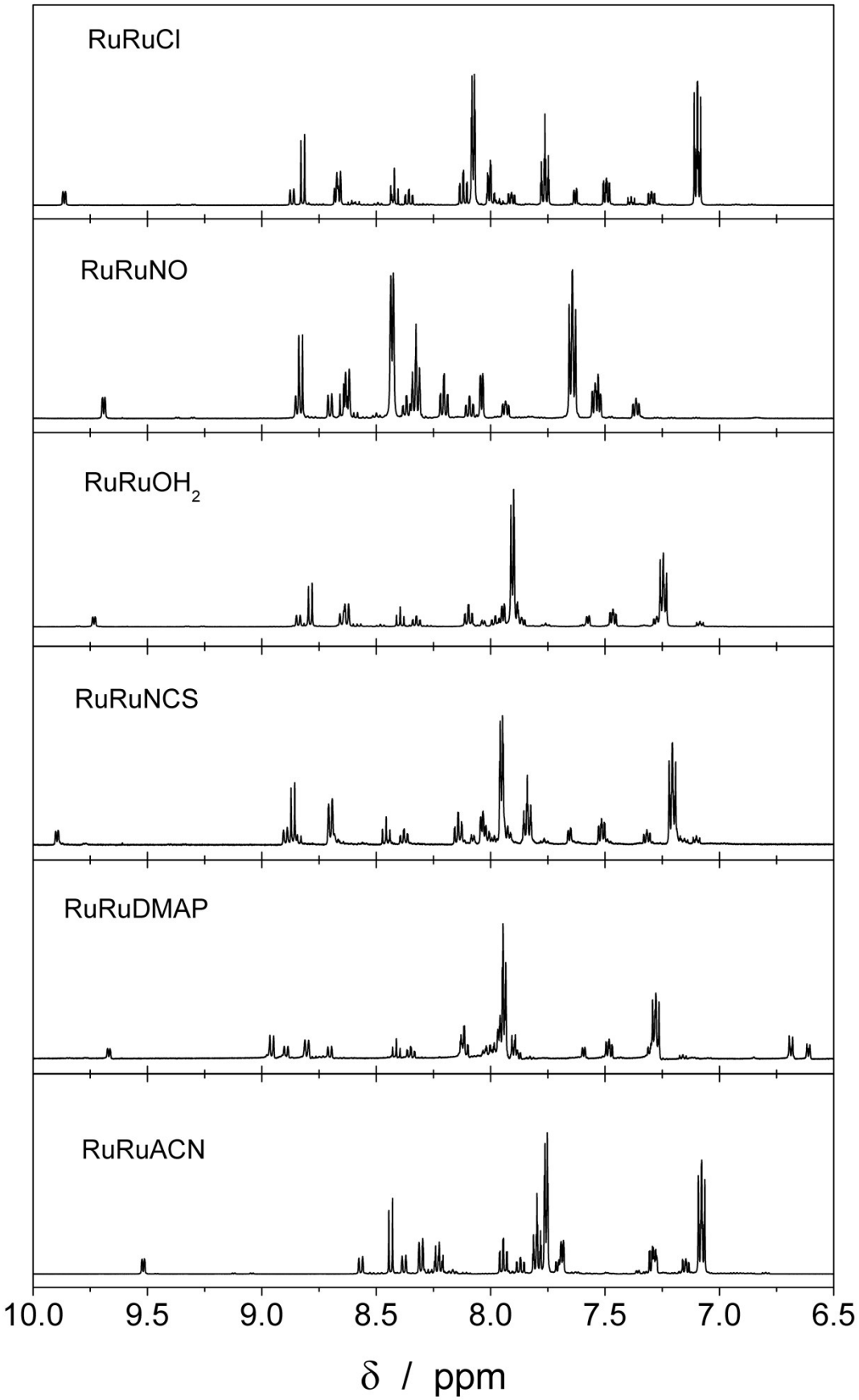

Figure S1. 500 MHz ^{1}H-NMR spectra of complexes **RuRuCl** (Acetone-D_6), **RuRuNO** (Acetone-D_6), **RuRuOH2** (Acetone-D_6), **RuRuNCS** (Acetone-D_6), **RuRuDMAP** (Acetone-D_6) and **RuRuACN** (Acetonitrile-D_3), from top to bottom.

Cyclic Voltammograms

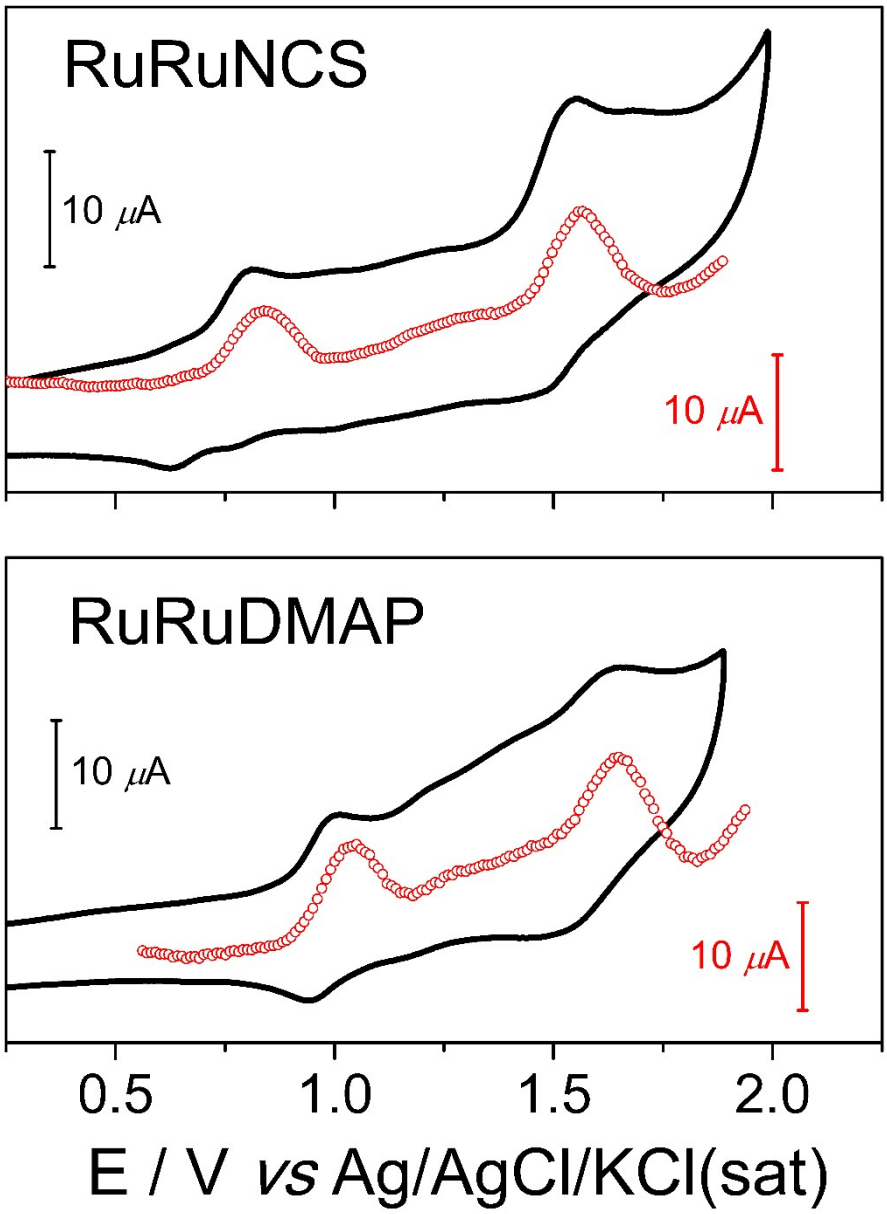

Figure S2. Cyclic voltammograms (solid line) and square wave voltammograms (voided circles) for the **RuRuNCS** y **RuRuDMAP** complexes in acetonitrile/0.1 M [TBA]PF_6.

VIS-NIR Spectroelectrochemistry

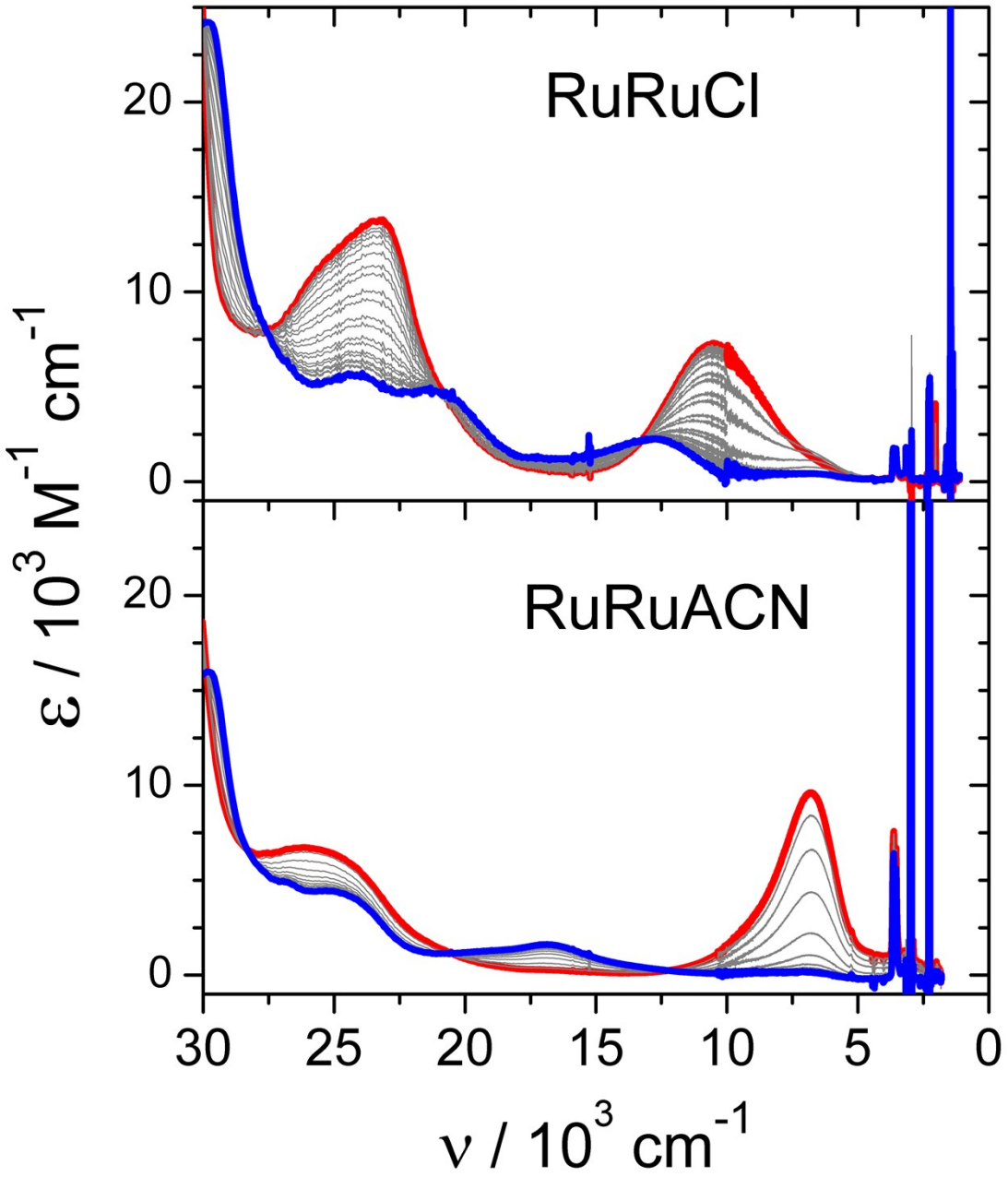

Figure S3. Vis−NIR spectroelectrochemistry for the **RuRuL** complexes in acetonitrile/0.1 M [TBA]PF_6, during the second oxidation processes. The spectra of the [II,III] (red), and [III,III] (blue) species are highlighted.

Solvent dependence of NIR bands

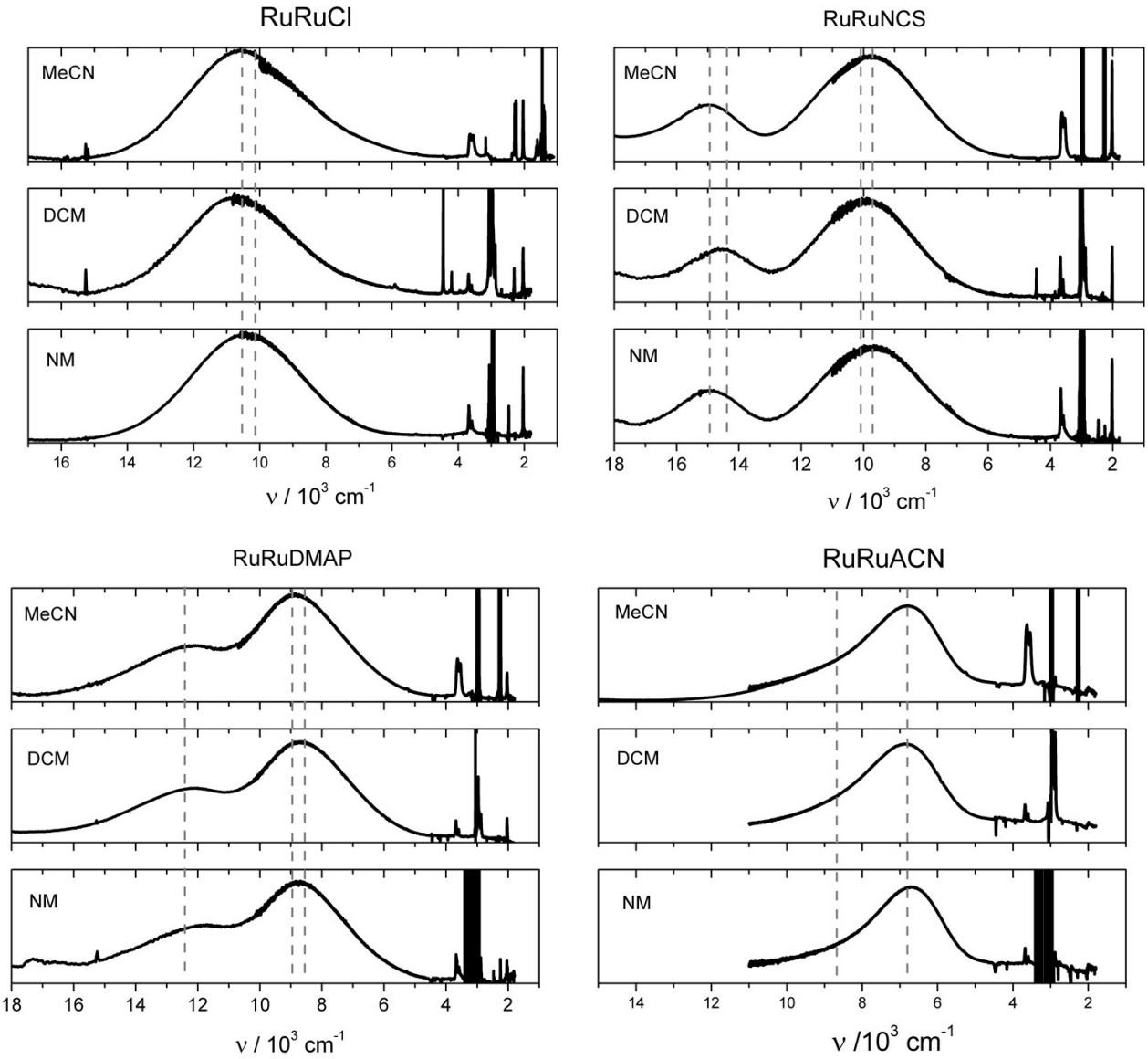

Figure S4. NIR absorption spectra for the **RuRuL** complexes in different solvents: acetonitrile (MeCN), dichloromethane (DCM) and nitromethane (NM).

IR Spectroelectrochemistry

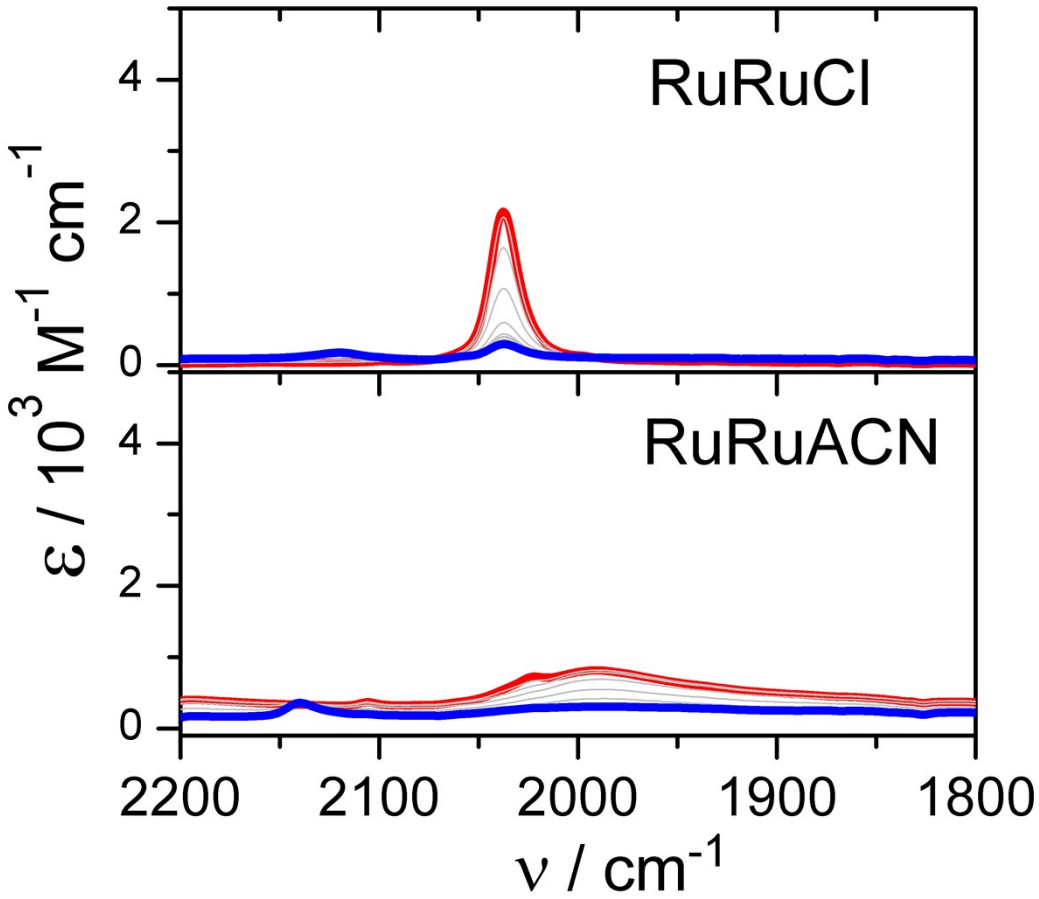

Figure S5. IR spectroelectrochemistry for the **RuRuL** complexes in acetonitrile/0.1 M [TBA]PF_6, during the second oxidation processes. The spectra of the [II,III] (red), and [III,III] (blue) species are highlighted.

DFT Calculations

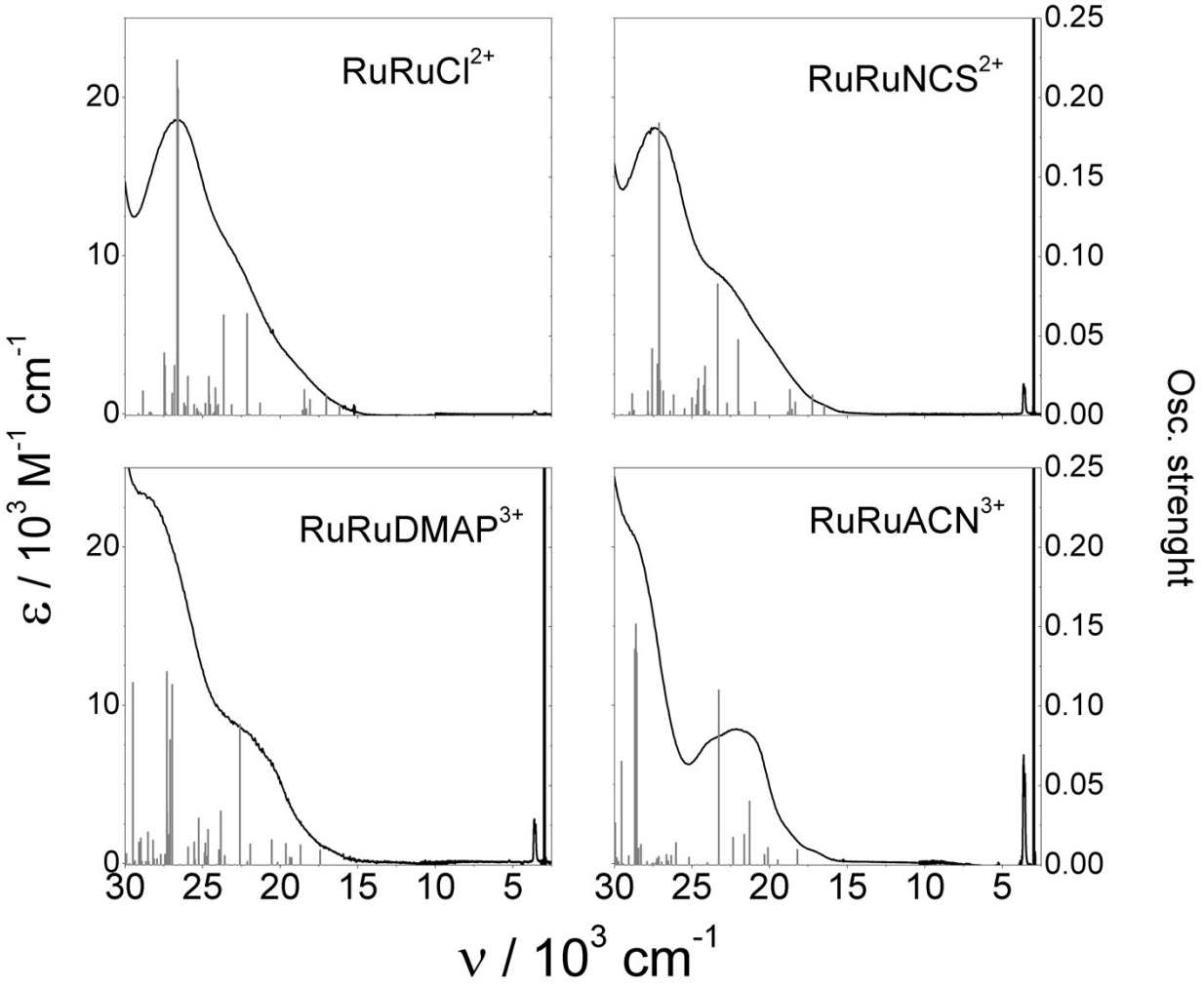

Figure S6. Comparison of the experimental vis-NIR spectra of the **RuRuL** complexes species in acetonitrile/0.1 M [TBA]PF_6 and the energy of the transitions calculated by (TD)DFT calculations (bars).

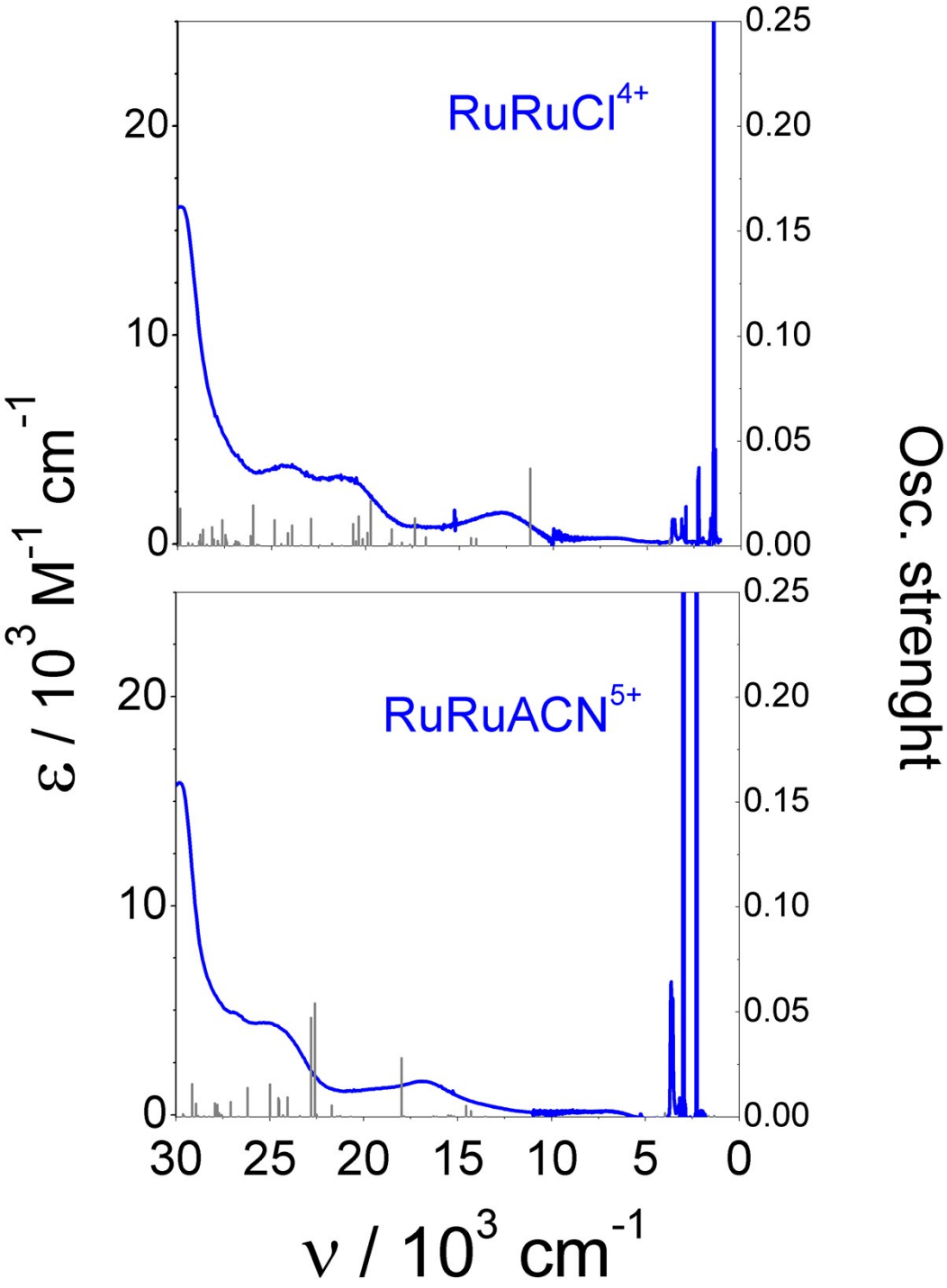

Figure S7. Comparison of the experimental vis-NIR spectra of the **RuRuL** complexes species in acetonitrile/0.1 M [TBA]PF_6 and the energy of the transitions calculated by (TD)DFT calculations (bars).

Table S3-A. Selected electronic transitions (f > 0.05) for the singlet **RuRuACN**$^{3+}$ ion calculated in MeCN

No.	Energy (cm^{-1})	Osc. Strength	Major contribs	Assignment
20	23285	0.1101	H-3 → L+1 (23%) H-3 → L+2 (49%) HOMO → L+2 (12%)	$d\pi_{xy}(Ru_{pp})$, $d\pi_{xz}(Ru_{py})$→ π*(tpy, bpy)
76	28580	0.1336	H-2 → L+6 (24%) HOMO → L+7 (37%) HOMO → L+8 (11%)	$d\pi_{xy}(Ru_{py})$, $d\pi_{xz}(Ru_{py}, Ru_{pp})$ → π*(py, tpy)
77	28632	0.1516	H-2 → L+5 (37%) H-2 → L+6 (17%) HOMO → L+8 (21%)	$d\pi_{xy}(Ru_{py})$, $d\pi_{xz}(Ru_{pp})$ → π*(py)
78	28687	0.1359	H-2 → L+5 (21%) H-2 → L+6 (15%) HOMO → L+8 (16%)	$d\pi_{xy}(Ru_{py})$, $d\pi_{xz}(Ru_{pp})$ → π*(py, tpy)

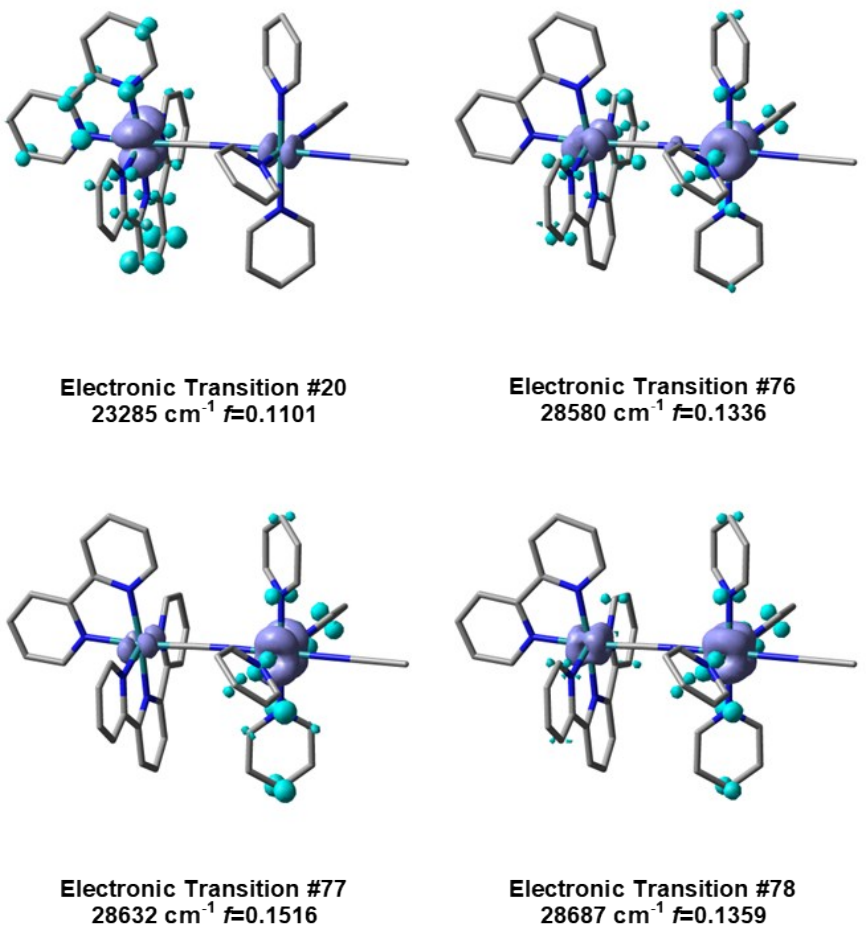

Figure S8-A. Electron density difference maps of the selected energy electronic transitions for the singlet **RuRuACN**$^{3+}$ ion. Purple indicates a decrease in charge density, while cyan indicates an increase.

Table S3-B. Selected electronic transitions (f > 0.05) for the singlet **RuRuDMAP**$^{3+}$ ion calculated in MeCN.

No.	Energy (cm^{-1})	Osc. Strength	Major contribs	Assignment
25	22612	0.0885	H-3 → L+1 (33%) H-3 → L+2 (40%)	$d\pi_{xy}(Ru_{pp}) \rightarrow \pi^*$(tpy, bpy)
71	26976	0.1135	H-2 → L+4 (39%) H-2 → L+5 (28%) H-2 → L+6 (11%)	$d\pi_{xy}(Ru_{py}) \rightarrow \pi^*$(py)
72	27100	0.0787	H-2 → L+4 (20%) H-2 → L+5 (36%) H-2 → L+7 (21%)	$d\pi_{xy}(Ru_{py}) \rightarrow \pi^*$(py)
77	27323	0.1216	H-6 → LUMO (15%) H-2 → L+3 (12%) H-2 → L+5 (11%) H-2 → L+6 (16%) H-2 → L+7 (18%)	$d\pi_{xy}(Ru_{py}) \rightarrow \pi^*$(py)
106	29511	0.1148	H-2 → L+22 (13%) H-1 → L+10 (24%) HOMO → L+12 (18%)	$d\pi_{xy}(Ru_{py}, Ru_{py}) \rightarrow \pi^*$(bpy, py)

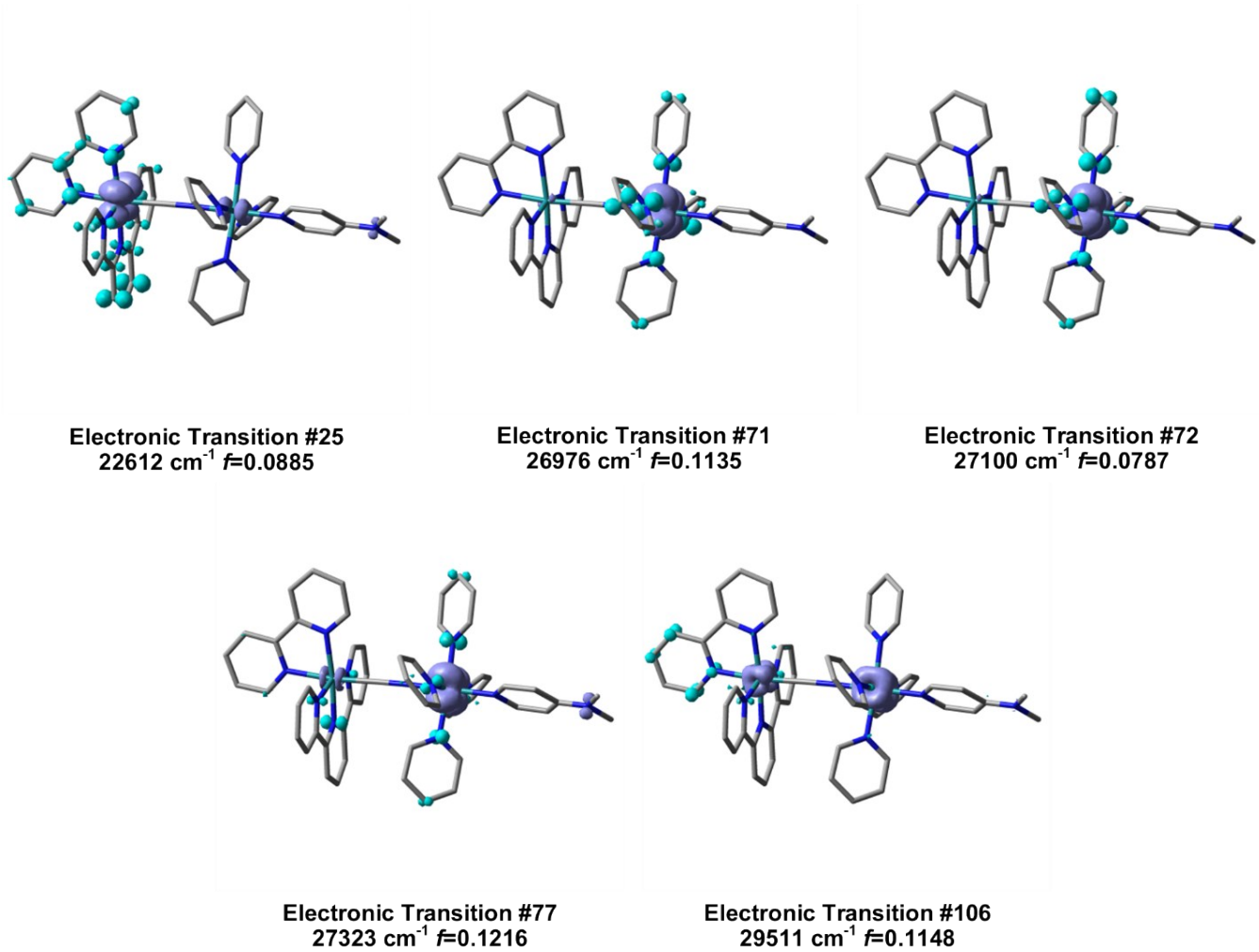

Figure S8-B. Electron density difference maps of the selected energy electronic transitions for the singlet **RuRuDMAP**$^{3+}$ ion. Purple indicates a decrease in charge density, while cyan indicates an increase.

Table S3-C. Selected electronic transitions (f > 0.05) for the singlet **RuRuNCS**$^{2+}$ ion calculated in MeCN.

No.	Energy (cm^{-1})	Osc. Strength	Major contribs	Assignment
37	23345	0.0828	H-4 → L+1 (78%)	$d\pi_{xy}(Ru_{pp}) \rightarrow \pi^*$(tpy, bpy)
79	27114	0.1611	H-2 → L+6 (46%) H-2 → L+7 (17%)	$d\pi_{xy}(Ru_{py}) \rightarrow \pi^*$(py)
80	27132	0.1840	H-2 → L+6 (28%) H-2 → L+7 (43%)	$d\pi_{xy}(Ru_{py}) \rightarrow \pi^*$(py)

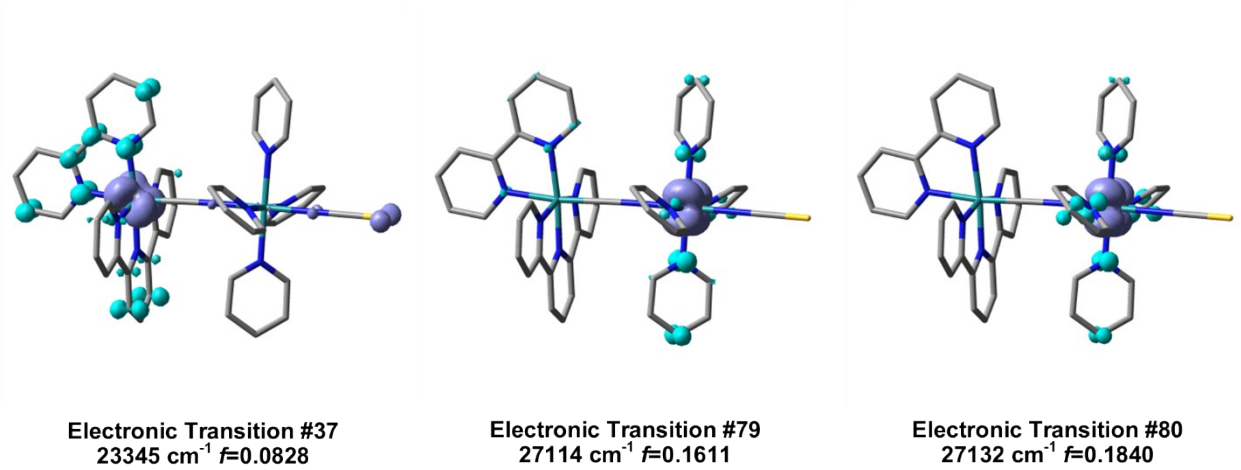

Figure S8-C. Electron density difference maps of the selected energy electronic transitions for the singlet **RuRuNCS**$^{2+}$ ion. Purple indicates a decrease in charge density, while cyan indicates an increase.

Table S3-D. Selected electronic transitions (f > 0.05) for the singlet **RuRuCl**$^{2+}$ ion calculated in MeCN.

No.	Energy (cm^{-1})	Osc. Strength	Major contribs	Assignment
31	22144	0.0639	H-3 → L+1 (63%) H-3 → L+2 (23%)	$d\pi_{xy}(Ru_{pp}) \rightarrow \pi^*$(tpy, bpy)
39	23649	0.0631	H-4 → L+1 (90%)	$d\pi_{yz}(Ru_{pp}) \rightarrow \pi^*$(tpy, bpy)
77	26596	0.2056	H-2 → L+6 (14%) H-2 → L+7 (32%) H-2 → L+8 (15%)	$d\pi_{xy}(Ru_{py}) \rightarrow \pi^*$(py)
78	26648	0.2236	H-2 → L+6 (32%) H-2 → L+7 (20%) H-2 → L+9 (15%)	$d\pi_{xy}(Ru_{py}) \rightarrow \pi^*$(py)

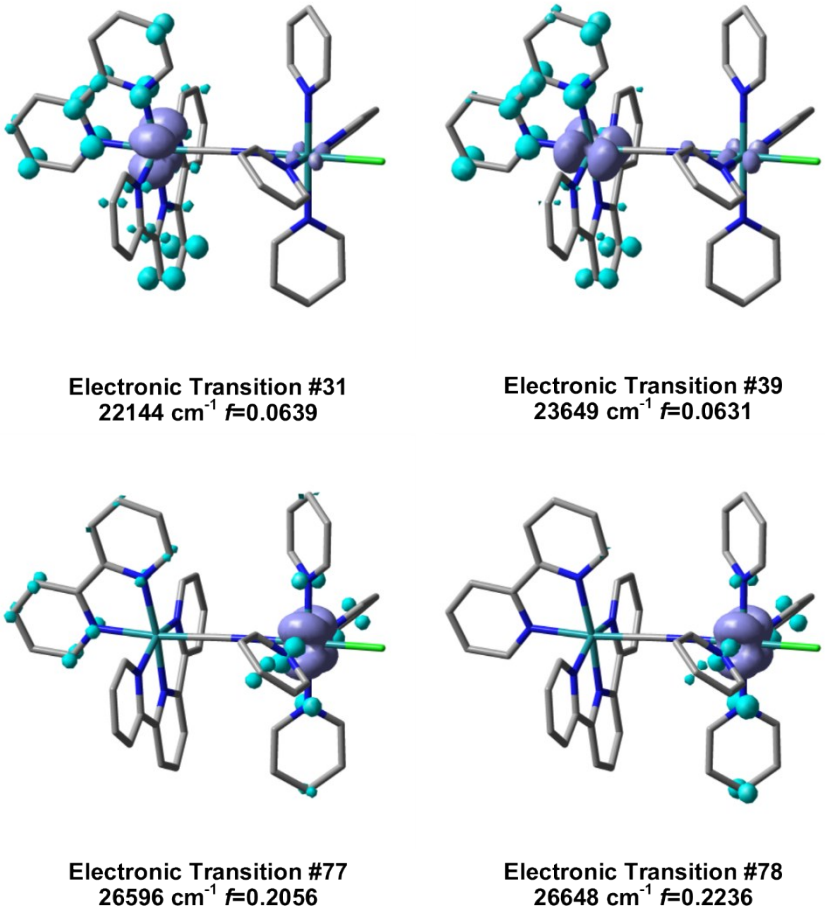

Figure S8-D. Electron density difference maps of the selected energy electronic transitions for the singlet **RuRuCl**$^{2+}$ ion. Purple indicates a decrease in charge density, while cyan indicates an increase.

Table S4-A. Selected electronic transitions for the doublet **RuRuACN^{4+}** ion calculated in MeCN.

No.	Energy (cm^{-1})	Osc. Strength	Major contribs	Assignment
1	932	0.0000	H-1β → LUMOβ (100%)	$d\pi_{xz}(Ru_{pp},Ru_{py}) \rightarrow d\pi_{yz}(Ru_{pp},Ru_{py})$
2	3147	0.0002	H-2β → LUMOβ (98%)	$d\pi_{xy}(Ru_{py}) \rightarrow d\pi_{yz}(Ru_{pp},Ru_{py})$
3	3655	0.0185	H-3β → LUMOβ (64%) HOMOβ → LUMOβ (34%)	$d\pi_{xy}(Ru_{pp}) \rightarrow d\pi_{yz}(Ru_{pp},Ru_{py})$
4	6932	0.2353	H-3β → LUMOβ (33%) HOMOβ → LUMOβ (64%)	$d\pi_{xy}(Ru_{py}) \rightarrow d\pi_{yz}(Ru_{pp},Ru_{py})$
5	7411	0.0005	H-4β → LUMOβ (96%)	$d\pi_{xz}(Ru_{pp},Ru_{py}) \rightarrow d\pi_{yz}(Ru_{pp},Ru_{py})$
6	14950	0.0050	H-5β → LUMOβ (91%)	$\pi(tpy) \rightarrow d\pi_{yz}(Ru_{pp},Ru_{py})$
7	15629	0.0009	H-6β → LUMOβ (92%)	$\pi(bpy) \rightarrow d\pi_{yz}(Ru_{pp},Ru_{py})$

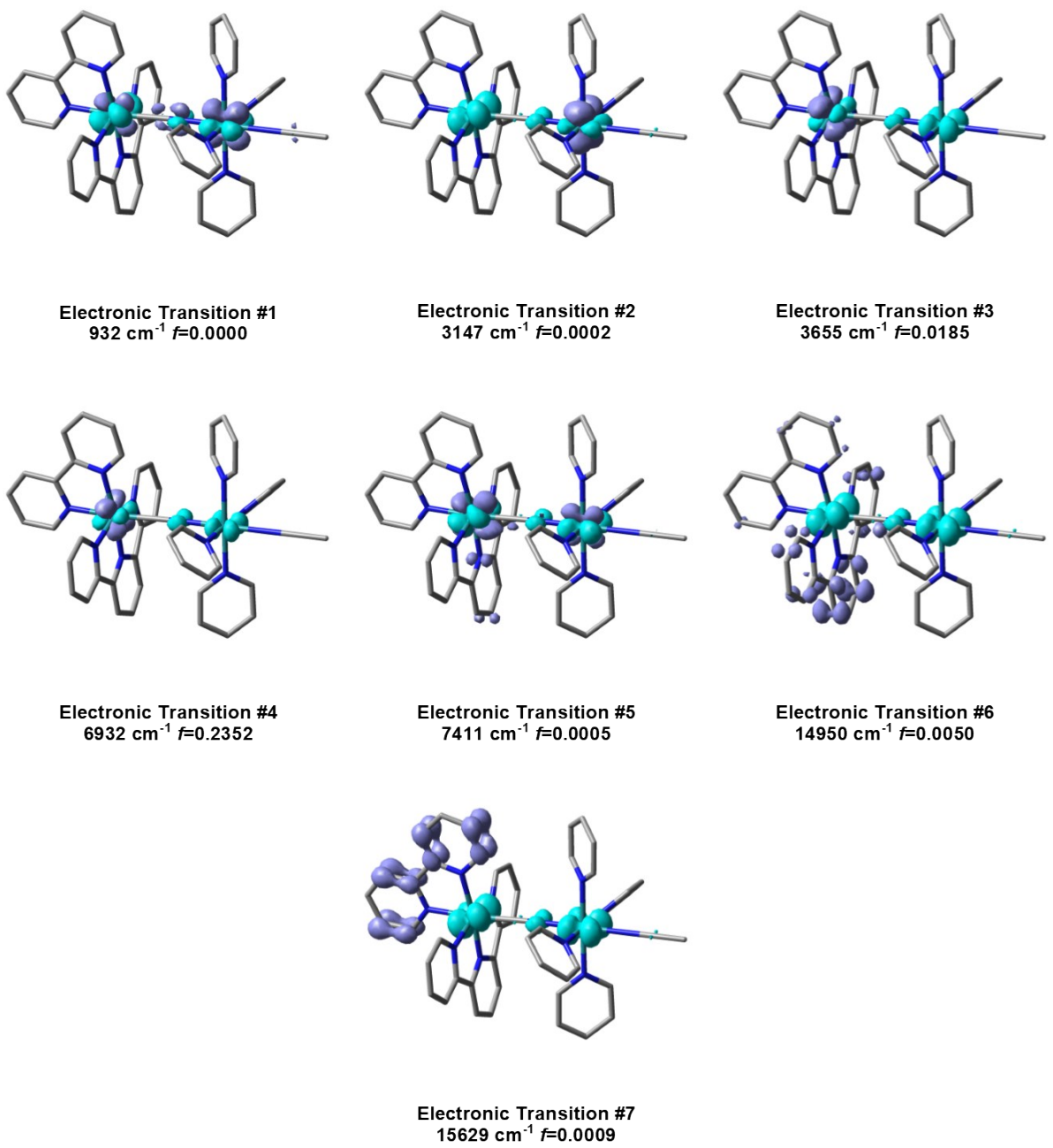

Figure S9-A. Electron density difference maps of the lowest energy electronic transitions for doublet **RuRuACN^{4+}** ion. Purple indicates a decrease in charge density, while cyan indicates an increase.

Table S4-B. Selected electronic transitions for the doublet **RuRuDMAP^{4+}** ion calculated in MeCN.

No.	Energy (cm^{-1})	Osc. Strength	Major contribs	Assignment
1	2099	0.0006	H-5β → LUMOβ (40%) H-2β → LUMOβ (30%) HOMOβ → LUMOβ (21%)	$d\pi_{xz}(Ru_{pp},Ru_{py}) \rightarrow d\pi_{yz}(Ru_{py})$
2	3735	0.0004	H-4β → LUMOβ (96%)	$d\pi_{xy}(Ru_{py}) \rightarrow d\pi_{yz}(Ru_{pp},Ru_{py})$
3	6642	0.0236	H-1β → LUMOβ (53%) HOMOβ → LUMOβ (42%)	$d\pi_{xy}(Ru_{pp})$, $d\pi y_{z}(Ru_{pp}) \rightarrow d\pi_{yz}(Ru_{py})$
4	7907	0.1896	H-2β → LUMOβ (11%) H-1β → LUMOβ (42%) HOMOβ → LUMOβ (34%)	$d\pi_{xy}(Ru_{pp})$, $d\pi_{yz}(Ru_{pp}) \rightarrow d\pi_{yz}(Ru_{py})$
5	8990	0.0745	H-5β → LUMOβ (38%) H-2β → LUMOβ (57%)	$d\pi_{xz}(Ru_{pp},Ru_{py}) \rightarrow d\pi_{yz}(Ru_{py},Ru_{pp})$
6	11108	0.0959	H-3β → LUMOβ (91%)	$\pi(DMAP) \rightarrow d\pi_{yz}(Ru_{py})$

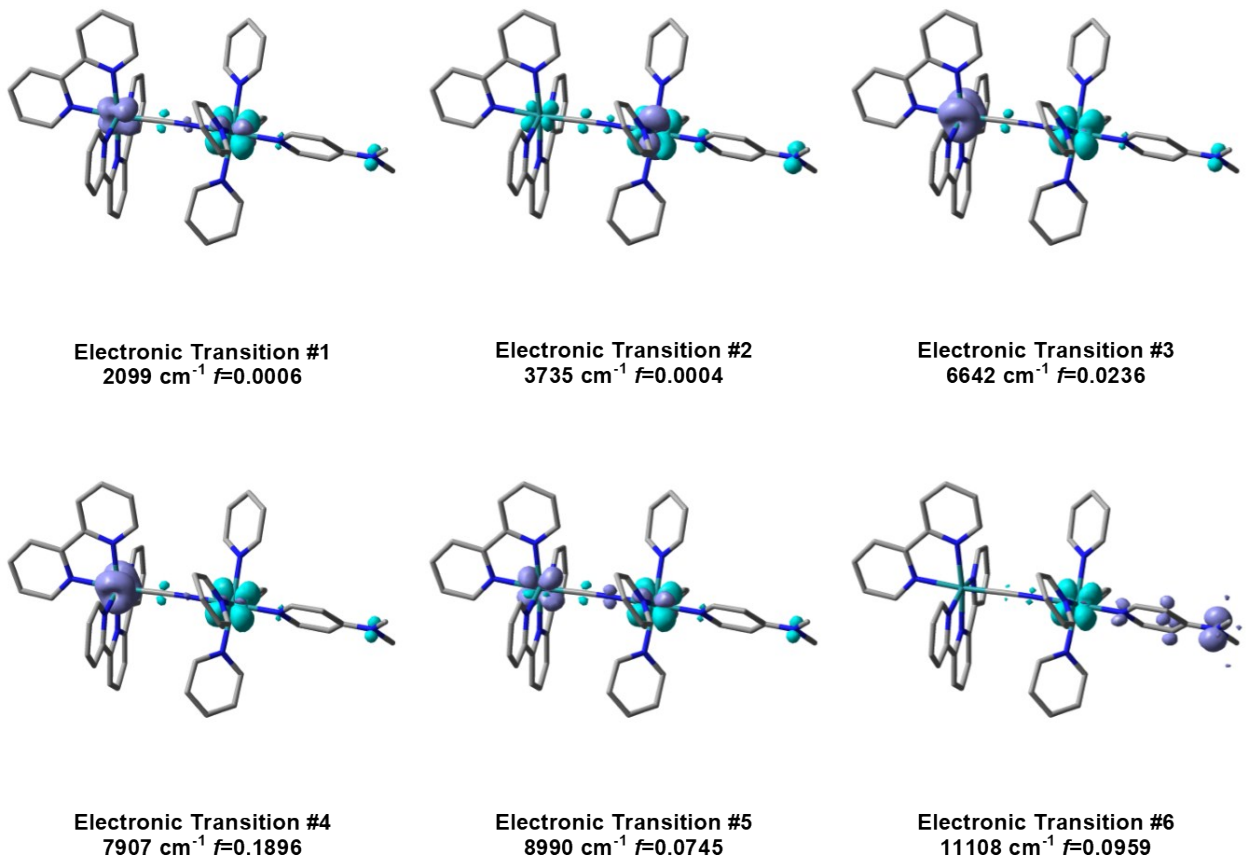

Figure S9-B. Electron density difference maps of the lowest energy electronic transitions for doublet **RuRuDMAP^{4+}** ion. Purple indicates a decrease in charge density, while cyan indicates an increase.

Table S4-C. Selected electronic transitions for the doublet **RuRuNCS^{3+}** ion calculated in MeCN.

No.	Energy (cm^{-1})	Osc. Strength	Major contribs	Assignment
1	592	0.0000	H-8β → LUMOβ (10%) H-1β → LUMOβ (12%) HOMOβ → LUMOβ (71%)	$d\pi_{xz}(Ru_{pp},Ru_{py}) \rightarrow d\pi_{yz}(Ru_{py},Ru_{pp})$
2	3751	0.0004	H-5β → LUMOβ (20%) H-4β → LUMOβ (76%)	$d\pi_{xy}(Ru_{py}) \rightarrow d\pi_{yz}(Ru_{py},Ru_{pp})$
3	7641	0.0349	H-2β → LUMOβ (27%) H-1β → LUMOβ (60%) HOMOβ → LUMOβ (11%)	$d\pi_{xy}(Ru_{pp}) \rightarrow d\pi_{yz}(Ru_{py})$
4	8794	0.1190	H-3β → LUMOβ (16%) H-2β → LUMOβ (63%) H-1β → LUMOβ (11%)	$d\pi_{xy}(Ru_{pp}) \rightarrow d\pi_{yz}(Ru_{py})$
5	9421	0.0655	H-3β → LUMOβ (75%) H-1β → LUMOβ (13%)	$d\pi_{xz}(Ru_{pp}) \rightarrow d\pi_{yz}(Ru_{py})$
6	13157	0.0000	H-8β → LUMOβ (85%)	$\pi(NCS) \rightarrow d\pi_{yz}(Ru_{py},Ru_{pp})$
7	13774	0.1148	H-5β → LUMOβ (76%) H-4β → LUMOβ (20%)	$\pi(NCS) \rightarrow d\pi_{yz}(Ru_{py},Ru_{pp})$

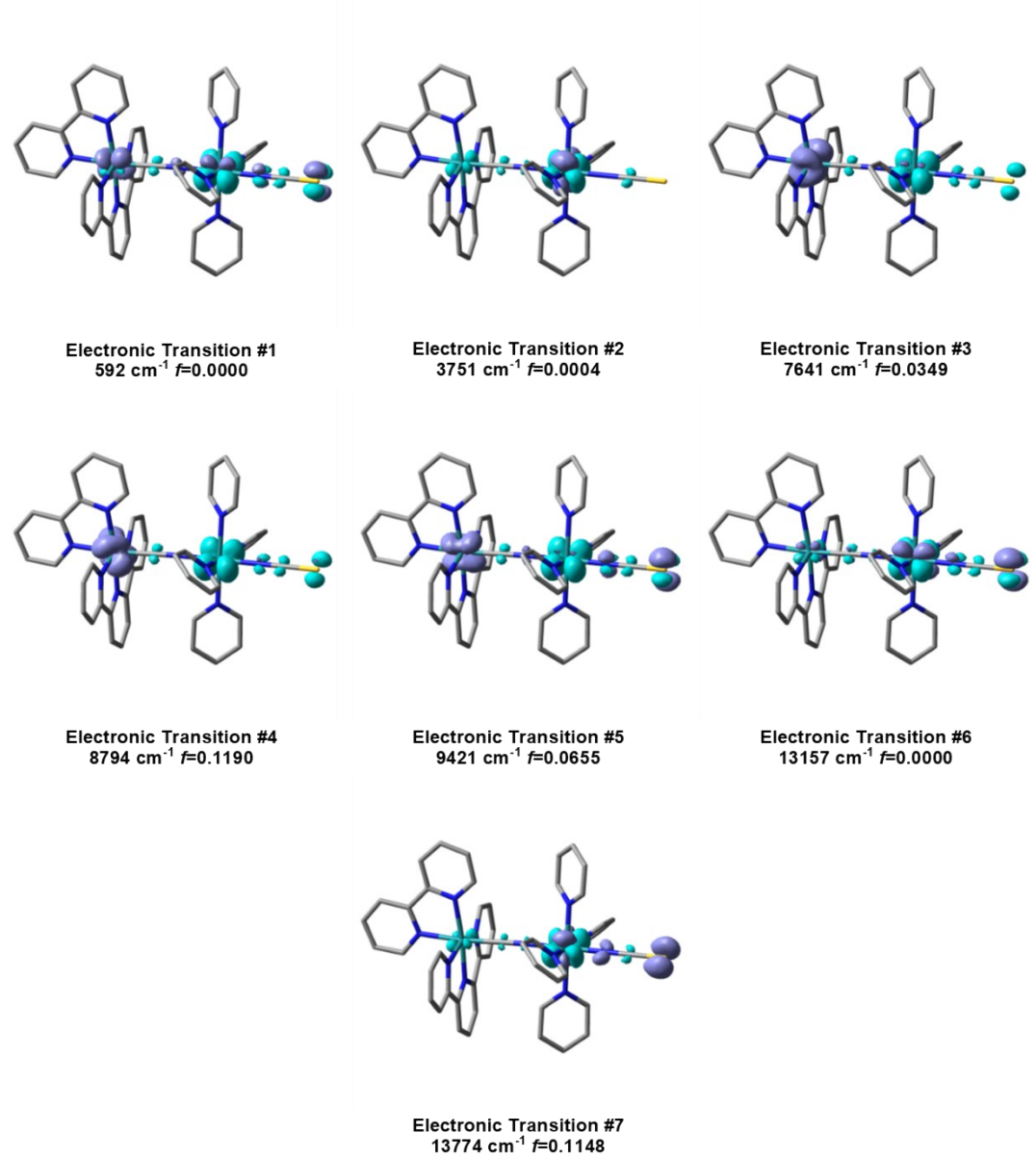

Figure S9-C. Electron density difference maps of the lowest energy electronic transitions for doublet **RuRuNCS^{3+}** ion. Purple indicates a decrease in charge density, while cyan indicates an increase.

Table S4-D. Selected electronic transitions for the doublet **RuRuCl^{3+}** ion calculated in MeCN.

No.	Energy (cm^{-1})	Osc. Strength	Major contribs	Assignment
1	771	0.0000	H-3β → LUMOβ (33%) H-1β → LUMOβ (10%) HOMOβ → LUMOβ (44%)	$d\pi_{yz}(Ru_{pp},Ru_{py}) \rightarrow d\pi_{xz}(Ru_{py})$
2	2622	0.0004	H-4β → LUMOβ (97%)	$d\pi_{xy}(Ru_{py}) \rightarrow d\pi_{xz}(Ru_{py},Ru_{pp})$
3	7998	0.0116	H-1β → LUMOβ (68%) HOMOβ → LUMOβ (28%)	$d\pi_{xy}(Ru_{pp}) \rightarrow d\pi_{xz}(Ru_{py})$
4	9382	0.0761	H-3β → LUMOβ (20%) H-2β → LUMOβ (39%) H-1β → LUMOβ (14%) HOMOβ → LUMOβ (24%)	$d\pi_{xz}(Ru_{pp})$, $d\pi_{yz}(Ru_{pp}) \rightarrow d\pi_{xz}(Ru_{py})$
5	10291	0.0681	H-3β → LUMOβ (38%) H-2β → LUMOβ (50%)	$d\pi_{xz}(Ru_{pp}) \rightarrow d\pi_{xz}(Ru_{py})$
6	18374	0.0021	H-5β → LUMOβ (67%)	$\pi(tpy) \rightarrow d\pi_{xz}(Ru_{py},Ru_{pp})$
8	18994	0.0105	H-7β → LUMOβ (80%)	$\pi(Cl) \rightarrow d\pi_{xz}(Ru_{py},Ru_{pp})$

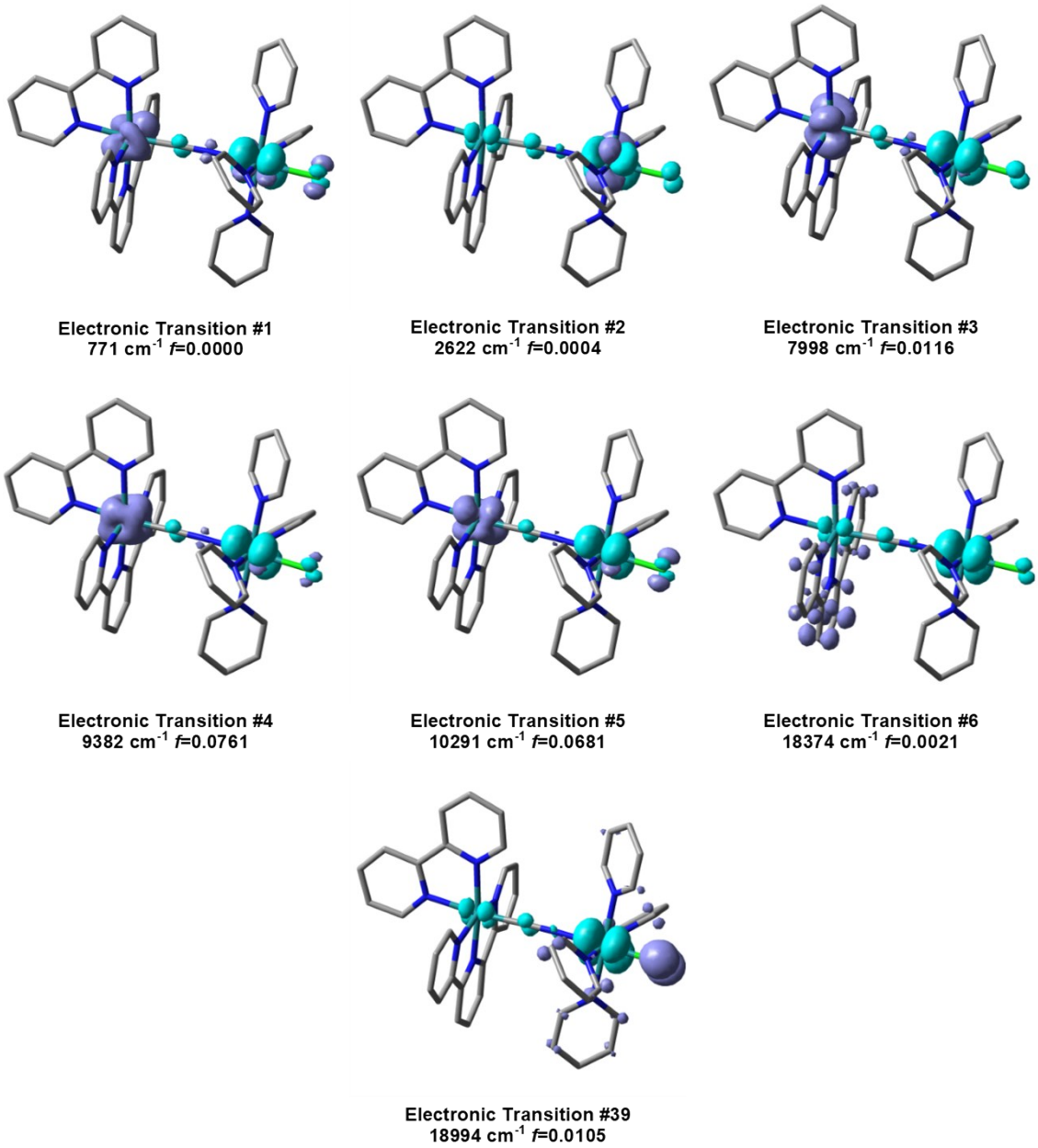

Figure S9-D. Electron density difference maps of the lowest energy electronic transitions for doublet **RuRuCl^{3+}** ion. Purple indicates a decrease in charge density, while cyan indicates an increase.

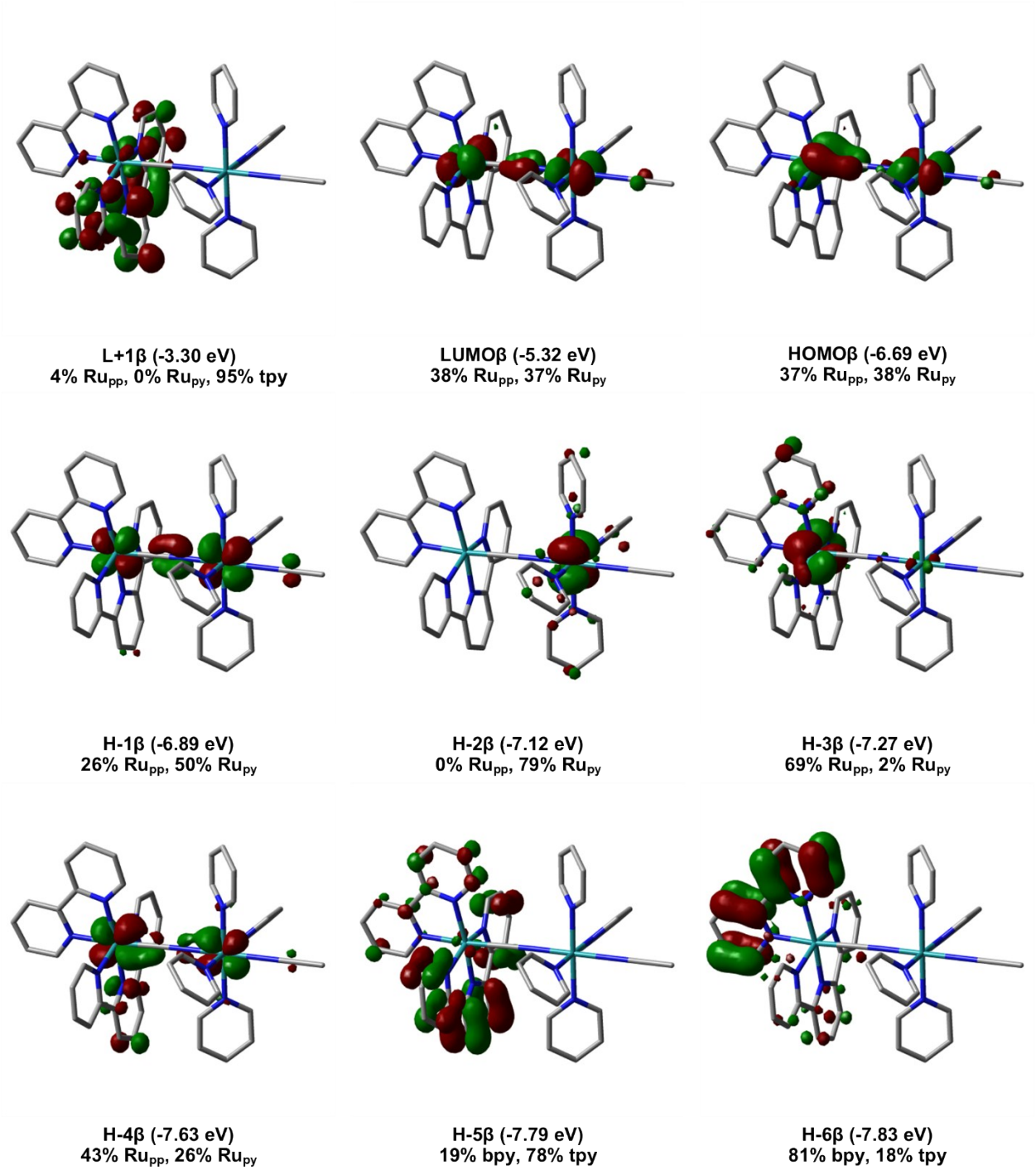

Figure S10-A. Computed β-orbitals for the doublet **RuRuACN^{4+}** ion calculated in MeCN.

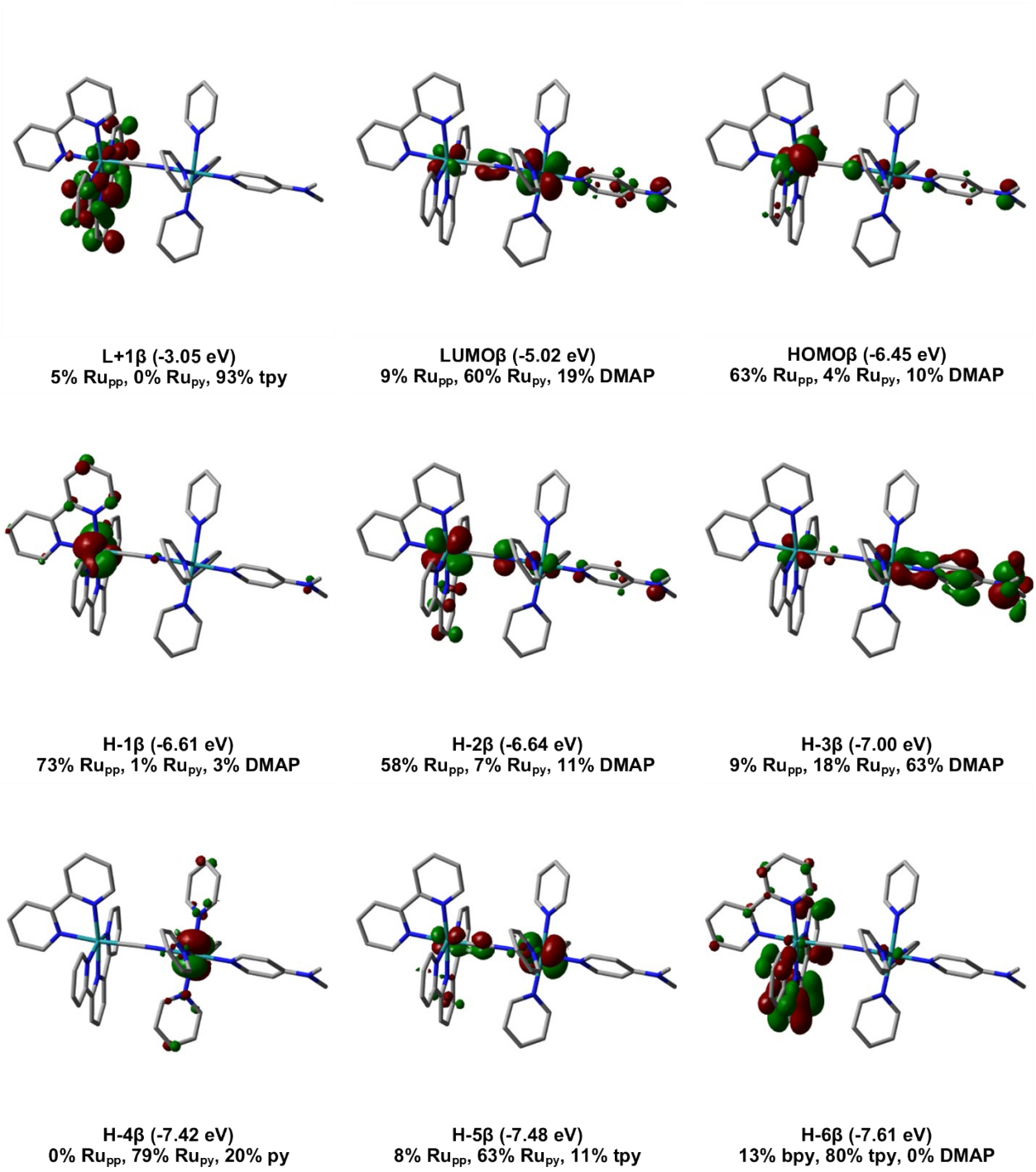

Figure S10-B. Computed β-orbitals for the doublet **RuRuDMAP^{4+}** ion calculated in MeCN.

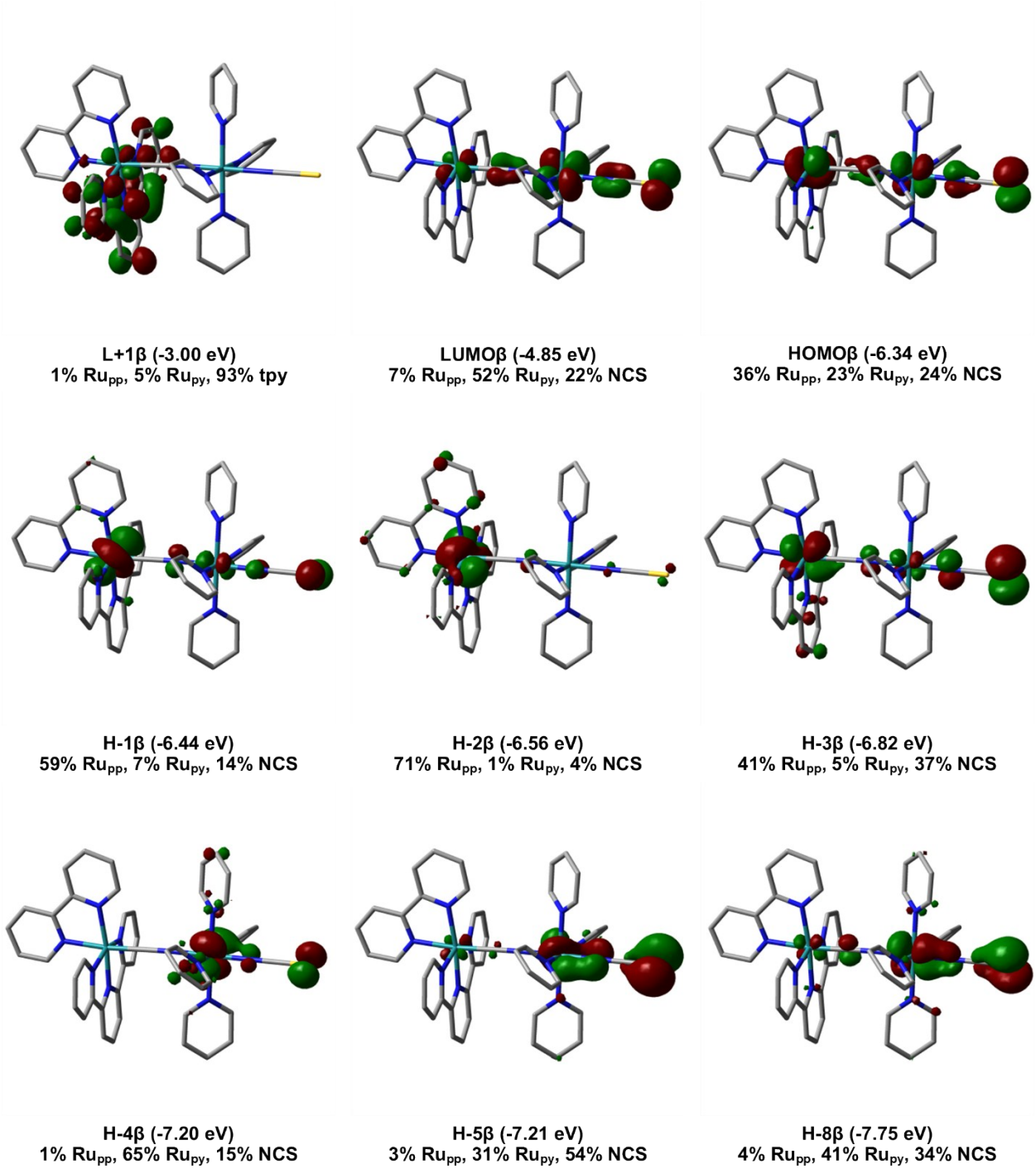

Figure S10-C. Computed β-orbitals for the doublet **RuRuNCS^{3+}** ion calculated in MeCN.

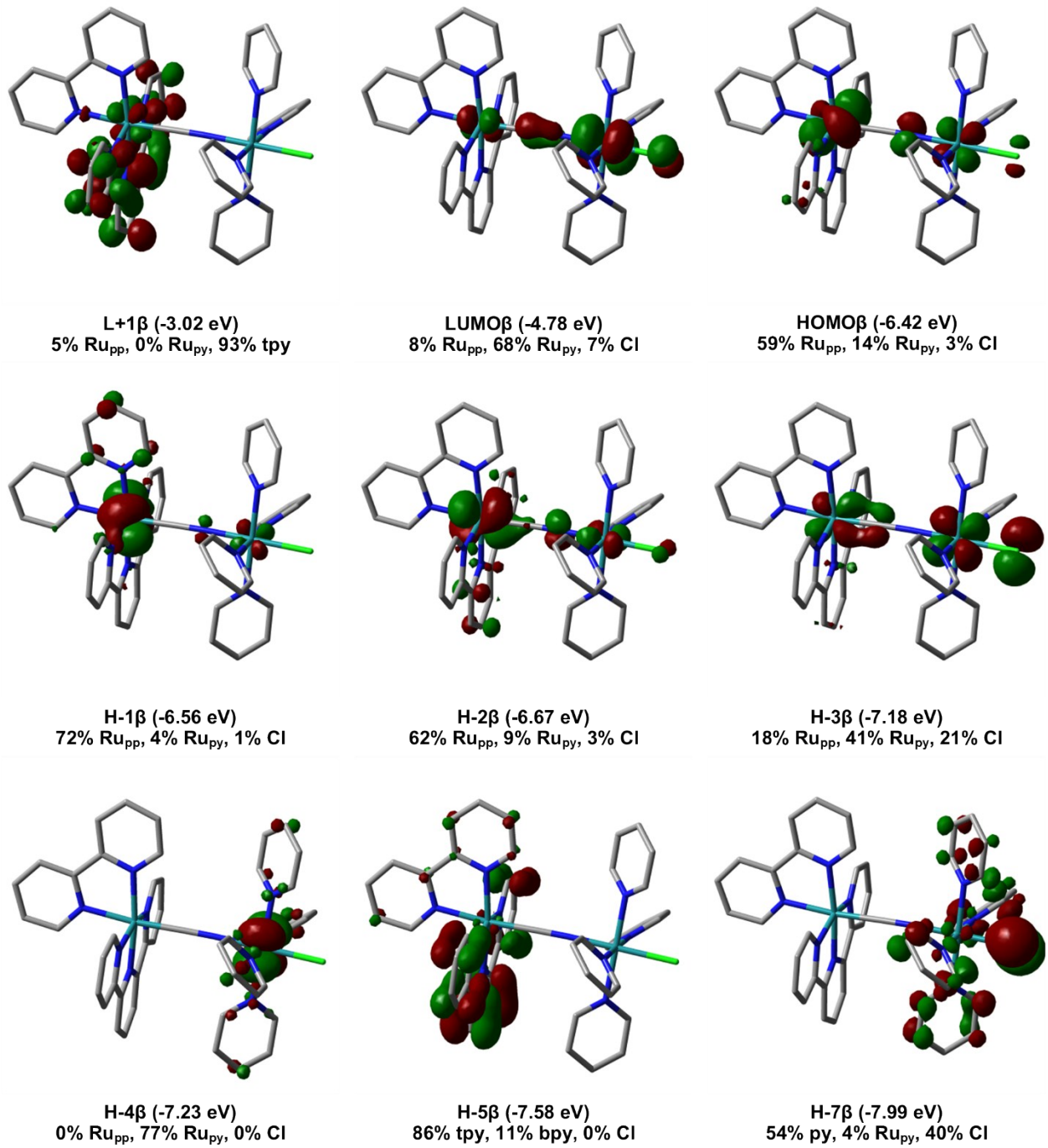

Figure S10-D. Computed β-orbitals for the doublet **RuRuCl^{3+}** ion calculated in MeCN.

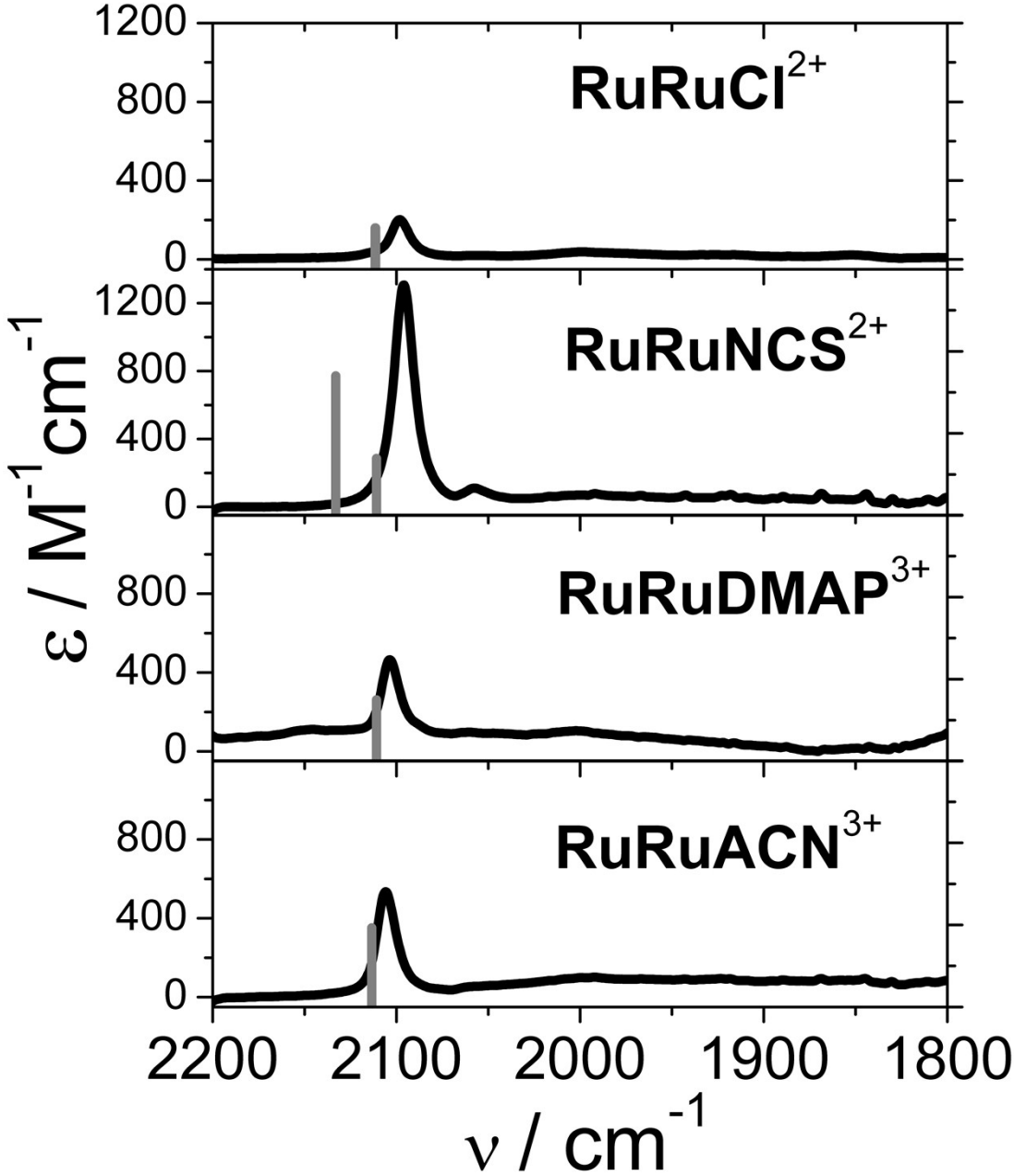

Figure S11. Comparison of the experimental IR spectra of the **RuRuL** complexes species in acetonitrile/0.1 M [TBA]PF_6 and the energy of the cyanide stretch calculated by (TD)DFT calculations (bars).

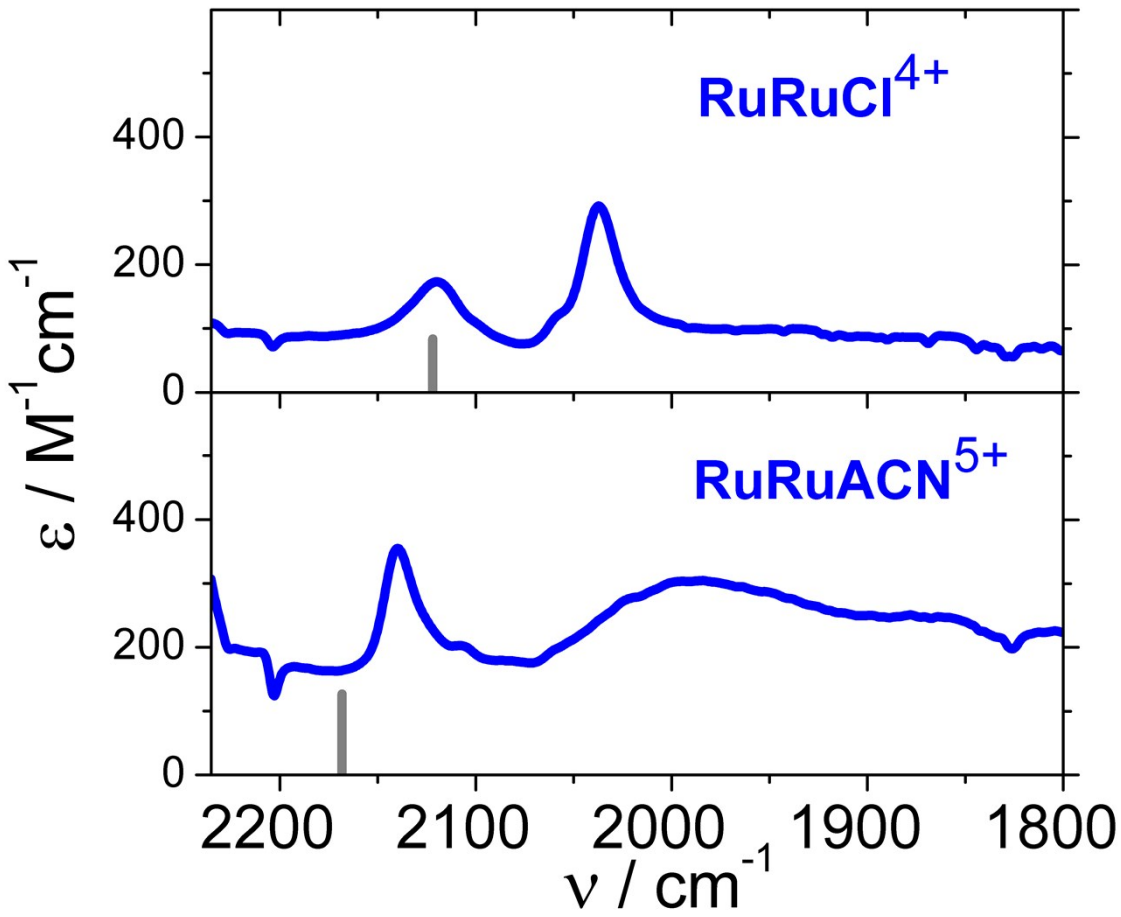

Figure S12. Comparison of the experimental IR spectra of the **RuRuL** complexes species in acetonitrile/0.1 M [TBA]PF_6 and the energy of the cyanide stretch calculated by (TD)DFT calculations (bars).

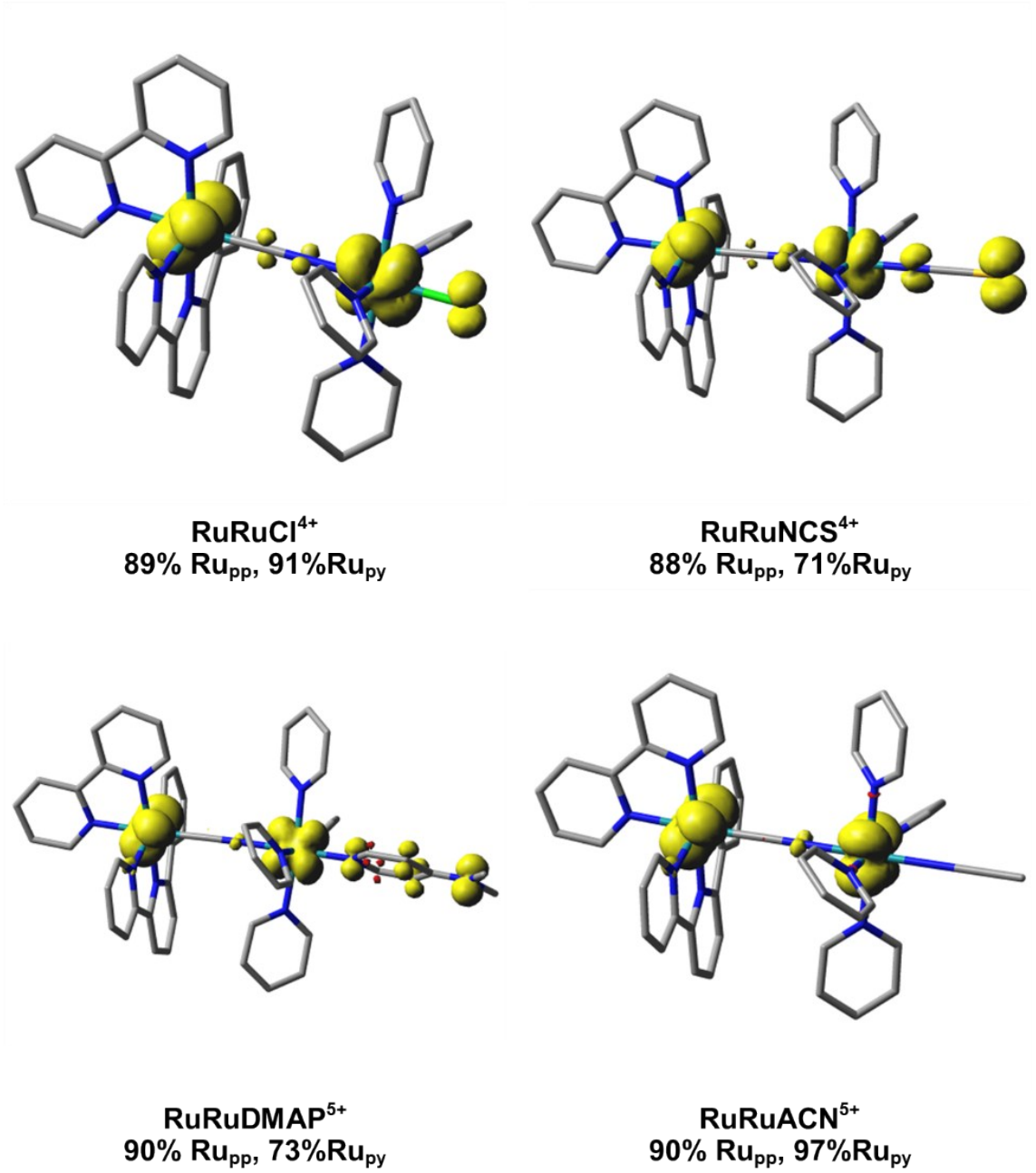

Figure S13. Computed spin density and Mulliken spin densities for the **RuRuL** (III,III) species.

Comparison between Ruthenium Polypyridines Siblings

Table S5. Energy and molar absorptivity of the IVCT transition the family of complexes [Ru(tpy)(bpy)(μ-CN)Ru(bpy)$_2$L)]$^{4/3+}$ and [Ru(tpy)(bpy)(μ-CN)Ru(py)$_4$L)]$^{4/3+}$.

	[Ru(tpy)(bpy)(μ-CN)Ru(bpy)$_2$L)]$^{4/3+}$ *		**[Ru(tpy)(bpy)(μ-CN)Ru(py)$_4$L)]$^{4/3+}$**	
L	ΔE / V	ν_{max} / 10^3 cm^{-1} (ε_{max} /10^3 M^{-1} cm^{-1})	ΔE / V	ν_{max} / 10^3 cm^{-1} (ε_{max} /10^3 M^{-1} cm^{-1})
Cl$^-$	0.83	10.8 (2.6)	0.87	10.4 (3.9)
SCN$^-$	0.63	9.5 (3.2)	0.75	9.7 (4.3)
DMAP	0.58	8.4 (4.0)	0.61	8.9 (7.5)
ACN	0.53	6.9 (9.3)	0.44	6.8 (9.5)

* Data extracted from Ref [2]

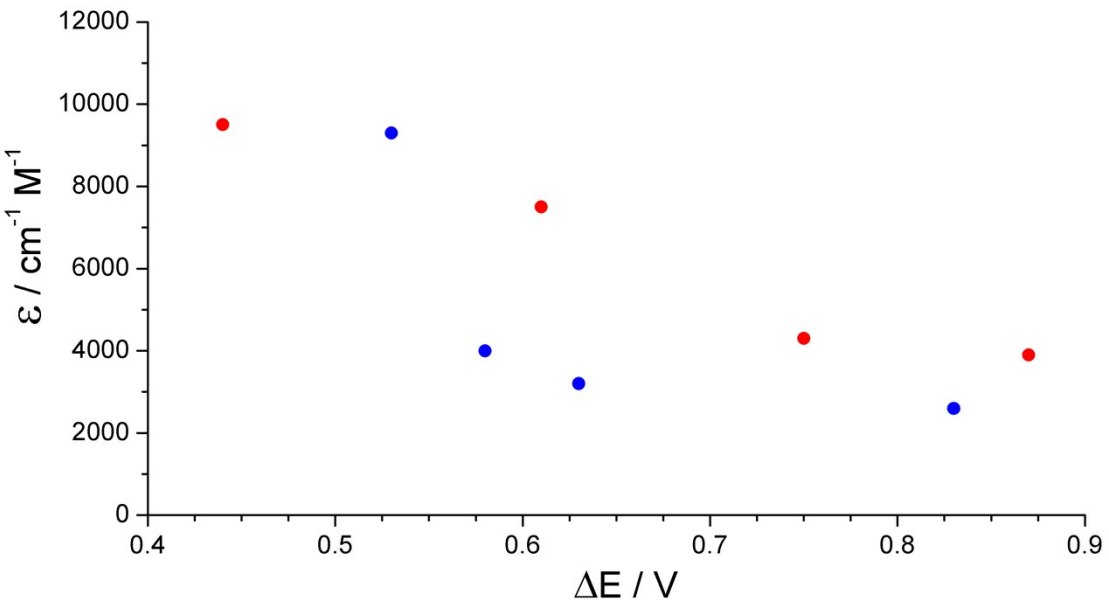

Figure S14. Dependence of the molar absorptivity of the IVCT transition with $\Delta E_{½}$ between the two redox couples for the family of complexes [Ru(tpy)(bpy)(μ-CN)Ru(bpy)$_2$L)]$^{4/3+}$ (blue) and [Ru(tpy)(bpy)(μ-CN)Ru(py)$_4$L)]$^{4/3+}$ (red).

References

(1) Cadranel, A.; Tate, J. E.; Oviedo, P. S.; Yamazaki, S.; Hodak, J. H.; Baraldo, L. M.; Kleiman, V. D. Distant Ultrafast Energy Transfer in a Trimetallic {Ru–Ru–Cr} Complex Facilitated by Hole Delocalization. *Phys. Chem. Chem. Phys.* **2017**, *19* (4), 2882–2893. https://doi.org/10.1039/C6CP06562G.

(2) Oviedo, P. S.; Pieslinger, G. E.; Cadranel, A.; Baraldo, L. M. Exploring the Localized to Delocalized Transition in Non-Symmetric Bimetallic Ruthenium Polypyridines. *Dalt. Trans.* **2017**, *46* (45), 15757–15768. https://doi.org/10.1039/C7DT02422C.